metals

MDPI

Article

Electrochemical Behaviour of PACVD TiN-Coated CoCrMo Medical Alloy

Suzana Jakovljević [1,*], Vesna Alar [2] and Antonio Ivanković [3]

[1] Department of Materials, Faculty of Mechanical Engineering and Naval Architecture, University of Zagreb, Ivana Lučića 5, 10002 Zagreb, Croatia

[2] Department of Welded Structures, Faculty of Mechanical Engineering and Naval Architecture, University of Zagreb, Ivana Lučića 5, 10002 Zagreb, Croatia; vesna.alar@fsb.hr

[3] Department of Electrochemistry, Faculty of Chemical Engineering and Technology, University of Zagreb, Marulic Square 19, 10002 Zagreb, Croatia; aivankovic8@gmail.com

* Correspondence: suzana.jakovljevic@fsb.hr; Tel.: +385-1-616-8391

Received: 27 April 2017; Accepted: 20 June 2017; Published: 23 June 2017

Abstract: CoCrMo alloys have been used in hip replacements for many years, and their properties can be enhanced with hard coatings. The TiN layer can be deposited on a CoCrMo alloy to its improve corrosion properties, such as reduction of the release of potentially harmful metal ions from CoCrMo-based surgical implants. In this work, a medical grade CoCrMo alloy was coated with TiN by means of plasma-assisted chemical deposition from the vapor phase (PACVD) technique at 500 °C for 4.5 h. The TiN/substrate interface and thickness of the TiN layer were analysed by scanning electron microscopy (SEM). Corrosion parameters E_{cor}, R_p, and I_{cor} were determined via direct current (DC) and alternating current (AC) electrochemical techniques. The SEM analysis showed a highly dense and quite uniform TiN layer, with a thickness of 2 µm. The results obtained by the DC electrochemical methods show better corrosion stability of the TiN/CoCrMo samples in comparison with CoCrMo in 0.9% NaCl at (25 ± 1) °C and (36 ± 1) °C. The electrochemical impedance spectroscopy (EIS) results show that there are nuclei on the TiN coating which reduce the corrosion stability.

Keywords: cobalt-chromium alloy; TiN; PACVD; electrochemical testing; scanning electron microscopy

1. Introduction

CoCrMo alloys, cobalt-based alloys, have been used in hip replacements due to their excellent mechanical properties, corrosion resistance, and good wear. These alloys are highly biocompatible materials [1–3] because of the presence of a spontaneously formed, extremely thin passive oxide layer on the alloy surface. The passive film on the CoCrMo alloys is composed mostly of Cr, followed by minor contents of Co and Mo oxides. These layers behave as a barrier to corrosion processes in the alloy [2,4,5], but there is still a concern about metal ions that are released from implants into the surrounding tissue in the body. The release of metal ions is an electrochemical process, and corrosion is a serious problem for medical metallic materials [6–8]. Investigation shows that the released metal ions are related with osteolysis, allergic reactions, and clinical implant failure [8,9].

The surface oxide layer on the CoCrMo alloy is not always stable in the human body, and therefore allows dissolution of metal ions. Pitting corrosion occurs when the passive film is locally severed due to chemical and mechanical processes. Pitting corrosion is a local dissolution leading to the formation of cavities in passive metals or alloys that are exposed to environments with aggressive ions (i.e., chlorides, bromides). Researchers have investigated the behaviour of CoCr pellets immersed in human serum, foetal bovine serum (FBS), synovial fluid, albumin in phosphate-buffered saline (PBS), and ethylenediaminetetraacetic acid (EDTA) in PBS [10]. The difference in the corrosive nature of

human serum, water, albumin in PBS, and synovial fluid after 5 days of immersion was highlighted by an oxide layer, which was respectively 15 nm, 3.5 nm, 1.5 nm and 1.5 nm thick.

The solution for preventing and reducing the dissolution of metal ions from implants and their release into the surrounding tissue is to coat the surface of the orthopaedic implant material. Coatings can improve the surface properties including wettability, hardness, friction coefficient, and wear of implants such as hip prostheses. Their limitations are adhesion to the substrate and their capacity in cyclic loading conditions [11]. Coatings with weak adhesion can delaminate from the surface of the substrate and expose the substrate to the body fluids allowing metal ions to be released into the surrounding tissue of the body causing allergic reactions. Partial delamination of the coating causes surface roughness and increases the wear of the tribopair. Delaminated hard coating flakes act as abrasive particles in contact with the surfaces and increase the wear rate. This is very important in tribological applications, such as hip joints, where a delaminated coating can cause a worse wear situation. The TiN coating is physiologically inert, non-toxic, and non-carcinogenic, and it is used in implantable devices approved by the FDA (Food and Drug Administration, Pittsburg, PA, USA) [12] The TiN coating is used for its excellent properties, such as great hardness, high decomposition temperature, and greater inertness to bodily fluids. The ceramic TiN layer reduces the release of metal ions into the patient's joint space, and minimizes bacterial proliferation [11]. The TiN coating is deposited on the CoCrMo alloy by PVD or laser deposition [11–15].

A thin coating of TiN was applied via Physical Vapour Deposition (PVD) in a previous study [16], due to the excellent biological properties of the TiN coating such as the reduction of the release of metal ions from the CoCrMo based surgical implants. Wisbey et al. investigated its corrosion performance using electrochemical techniques and atomic absorption analysis. The release of cobalt and chromium ions was shown to be reduced by the presence of the TiN coating.

Goldberg and Gilbert [17] investigated the mechanical and electrochemical behaviour of passivated and TiN/AlN-coated surfaces of CoCrMo and Ti6Al4V alloys. This behaviour was investigated in one group of CoCrMo and Ti6Al4V alloy samples passivated with nitric acid, and another group coated (via PVD) with a novel TiN/AlN coating. In this study, aerated phosphate buffered saline (PBS) at pH = 7 was used for all electrochemical test procedures. This study found that the oxide coatings provide increased corrosion resistance to the substrate alloys.

Bolton and Hu [18] investigated the electrochemical behaviour of three PVD coatings, CrN, TiN, and diamond like carbon (DLC), applied to a wrought high carbon CoCrMo alloy substrate material. Results in this study showed that all three coatings produced significant improvements in corrosion resistance compared to the performance of the wrought cobalt alloy, but that some corrosive attack to both the CrN and TiN coatings occurred, and some risk of attack to the cobalt alloy substrate existed due to the coating defects or when damage to the coating occurred.

Dicu et al. [19] investigated the corrosion resistance of titanium oxide thin layers deposited by Metal Organic Chemical Vapor Deposition (MOCVD) on a CoCr alloy substrate. The corrosion test was cyclic voltammetry, and it was performed in artificial saliva as the test solution.

Researchers have shown that a TiN coating on a CrCo alloy prevents corrosion attack. Previous studies have investigated the electrochemical behaviour of PVD [17,18] or CVD [19] coated TiN layers on CoCrMo alloys. However, researchers have not investigated the tribomechanical or electrochemical behaviour of a PACVD-coated TiN coating on a surgical grade CoCrMo alloy. The PACVD process is one of the innovative processes in surface engineering. The procurement of a new PACVD device enables the production of various thin mono-, multi-, nano-, and gradient-layered coatings—such as TiN, TiCN, TiAlN, TiBN, etc.

The aim of the present research was to investigate the electrochemical behaviour of PACVD-coated TiN layers on a medical grade CoCrMo alloy. This study combines the use of scanning electron microscopy (SEM), energy dispersion spectroscopy (EDS), and direct current (DC) and alternate current (AC) electrochemical techniques.

2. Materials and Methods

A spherical medical grade CoCrMo alloy (ASTM F75) was the base material with nominal compositions of 27.77% Cr, 5.56% Mo, and balanced Co (all in wt %). The substrate materials were spherical heads of hip endoprostheses with a diameter of 3.0 cm. All the samples were mounted in the DF-3 device—OTEC (OTEC Präzisionsfinish Gmbh, Karlsruhe, Germany), wet-polished with conical plastic grinding chips KM added with a SC15 compound, and then dry-finished by M5 corn granulate (grain size 0.8–1.3 mm) impregnated with a PP 04 polishing powder for high-quality, smooth, mirror-finish surfaces of the implants. The samples were ultrasonically cleaned in 70% ethyl alcohol for 90 s at 22 °C, dried, and stored in a desiccator. TiN coatings were produced by a plasma-assisted chemical deposition from the vapor phase (PACVD) process in an industrial furnace Type PC 70/90 RÜBIG (RÜBIG GmbH & Co KG, Marchtrenk, Austria) with a hot wall. Before the deposition, hip heads were heated to the temperature of 420 °C and the pressure of 2 mbar, and cleaned with argon and hydrogen to remove impurities. The deposition was carried out in Ar, H_2, $TiCl_4$, and N_2 atmosphere at the constant pressure of 2 mbar, with the substrate temperature of 500 °C and discharge voltage of 490 V. The deposition time was 4.5 h. TiN-coated CoCrMo hip heads were cut into quarters for various characterization techniques.

Scanning electron microscopy analyses were performed using a TESCAN VEGA 5136 mm system (TESCAN Brno, Brno, Czech Republic) to analyse the coating/substrate interface and to determine the coating thickness. The elemental analyses of the samples were carried out by Energy Dispersive Spectroscopy (Oxford Instruments, Belfast, UK) on the SEM.

The CoCrMo substrate and TiN/CoCrMo samples were studied by direct current and alternating current techniques in a solution of 0.9% NaCl at (25 ± 1) °C and (36 ± 1) °C. Corrosion parameters such as the corrosion potential (E_{corr}), corrosion current density (j_{corr}), and polarization resistance (R_p) were obtained using the standard three-electrode system. The capacity of the polarisation electrochemical cell used was 1000 mL. The working electrode of the CoCrMo specimens was polished with emery paper 600, and then washed in distilled water and degreased in ethyl alcohol, but the samples of CoCrMo with a TiN layer were only degreased in ethyl alcohol before use. The counter electrode was graphite, and the reference electrode was a saturated calomel electrode.

Electrochemical impedance spectroscopy (EIS) measurements were carried out with AMETEK, Princeton Applied Research, VersaSTAT3 model device (AMETEK Scientific 131 Instruments, Princeton applied research, Berwyn, PA, USA). Before the beginning of the impedance measurements, the samples were immersed for one hour in an electrolyte solution in order to establish a corrosion equilibrium potential (for CoCrMo, −700 mV at 25 °C and −240 mV at 36 °C; for TiN/CoCrMo, −592 mV at 25 °C and −190 mV at 36 °C). Electrochemical and corrosion behaviours with and without a coating were tested in 100 mL of 0.9% NaCl solution at 25 ± 1 °C and 36 ± 1 °C. The exposed area of each sample was approximately 1 cm^2. The experimental testing comprised the three-electrode electrochemical system which contained a working electrode, a saturated calomel electrode and a graphite stick as a counter electrode. The AC amplitude of the excitement signal was 10 mV, and the measurements were carried out in the frequency range between 100 kHz and 1 mHz. The obtained data were analysed with the ZSimpWin Version 3.2 software (AMETEK Scientific Instruments, Princeton applied research, Berwyn, PA, USA). The impedance data were obtained as the function of the frequency and variable voltage. The analysis includes the application of a typical impedance model for the surfaces of electrodes with and without a coating, and the curves were obtained with a non-linear method of the smallest squares in the ZSimpWin Version 3.2 software. The standard circuit model for a surface without a coating (Randles circuit) is modified, and contains a constant phase element (CPE) at the place where the capacity element does not show pure capacity behaviour of the interface. The CPE impedance is given with the relation $Z = 1/((i\omega)^a Q)$, where Q is the capacity element, ω is the frequency, i is the imaginary number, and a is the exponent between 0 and 1 (if $a = 1$, the system behaves as an ideal capacitor, and if $a = 0$, it behaves as an ideal resistor). It is well-known that the coating properties, such as surface roughness, porosity, and similar properties [20,21], influence the CPE. Statistical analysis of the data included the F-test and T test.

3. Results and Discussion

3.1. SEM and EDS Results

In the present study, SEM and EDS analyses were carried out on one of the coated samples and the results are shown in Figures 1 and 2.

Figure 1a is a cross section of the TiN coating/CoCrMo substrate, and it demonstrates a great defined interface between the coating and the substrate. The cross-sectional view presents a highly dense and quite uniform TiN layer and good adhesion between the coating and the substrate. The coating thickness is 2 µm. The image given in Figure 1b presents the surface morphology of the TiN layer and it shows some surface defects—micro-metal (TiN) droplets on the coating surface. These droplets may be potential places for corrosive attacks in the TiN coating which enable the corrosive environment to penetrate the CoCrMo substrate. Figure 2 shows the EDS results for one of the TiN-coated samples.

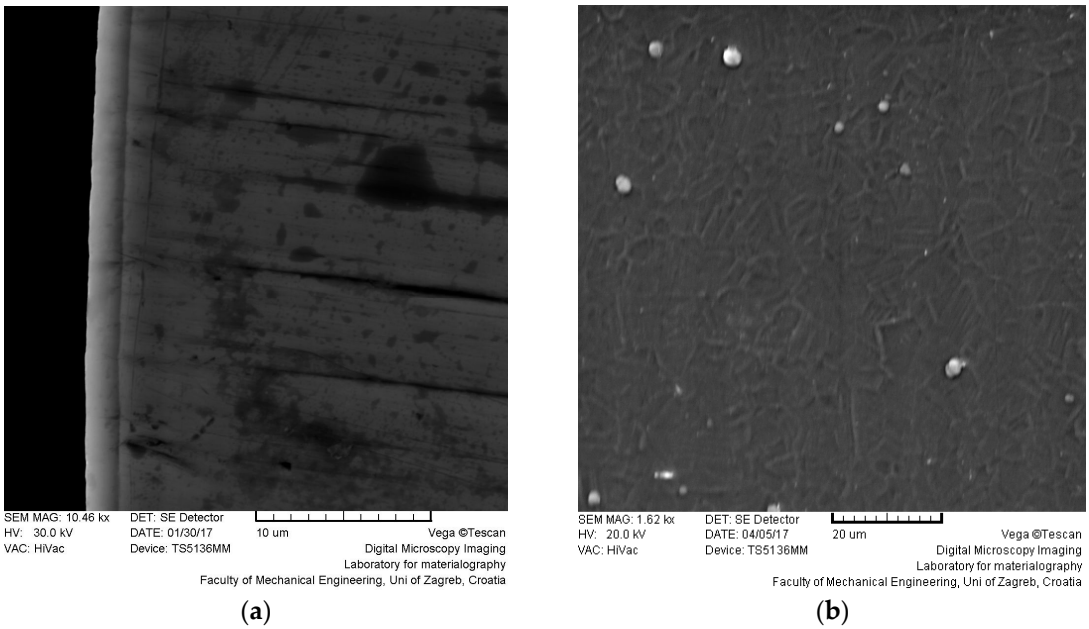

Figure 1. SEM image: (**a**) a cross-section of the TiN coating/CoCrMo substrate; (**b**) surface morphology of the TiN-coated substrate.

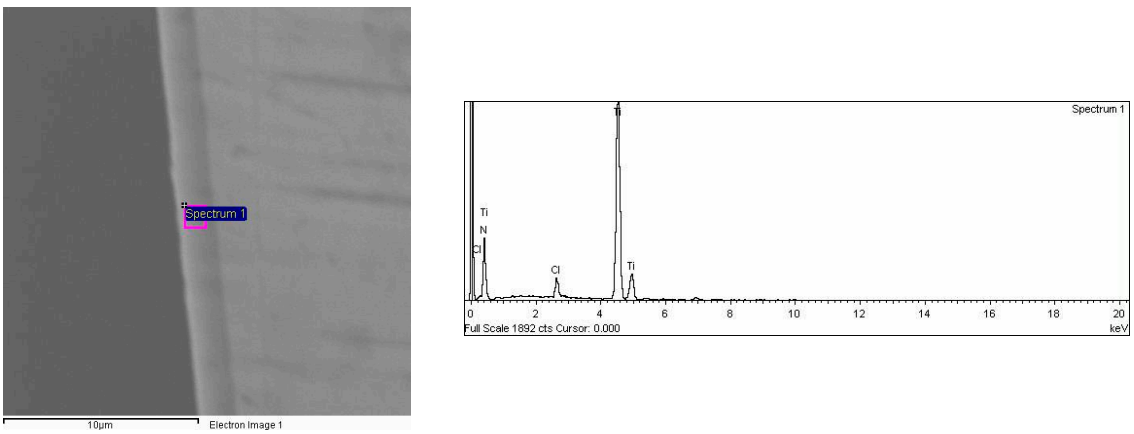

Figure 2. *Cont.*

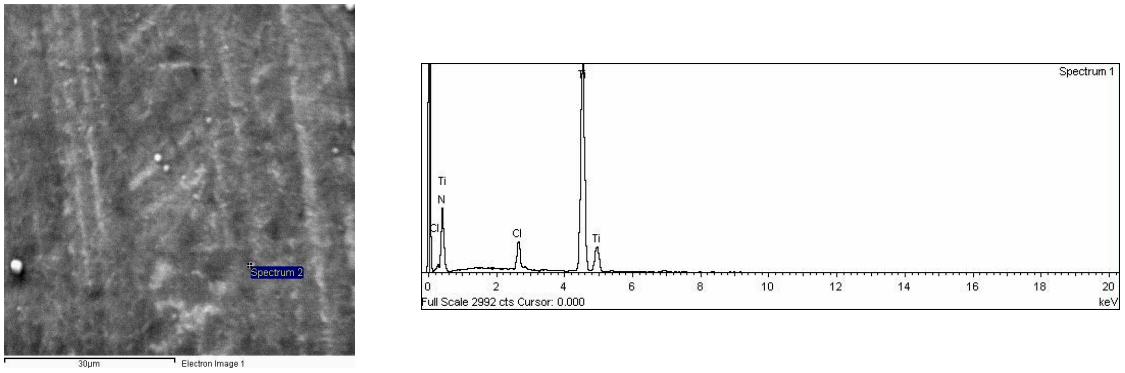

(**b**)

Figure 2. The energy dispersion spectroscopy (EDS) analysis of: (**a**) the TiN layer; (**b**) droplets on the surface of the TiN-coated substrate.

The EDS analysis given in Figure 2a presents the chemical composition of the coating. The analysis shows that the layer contains three elements: Ti, N, and Cl. The chlorine present in the spectrum is from the precursor ($TiCl_4$) from the PACVD procedure of the coating deposition. Figure 2b shows the EDS analysis of the droplets on the film surface which shows titanium and nitrogen peaks that indicate that the droplets are TiN micro-metal droplets.

3.2. Electrochemical DC Results

The results of the electrochemical DC techniques, corrosion potential E_{corr}, corrosion current density (j_{corr}) and polarization resistance (R_p), corrosion rate (v_{cor}), and efficient protection (η) are presented in Table 1. DC electrochemical testing was used to determine the corrosion current density of the substrate and the TiN coating on the CoCrMo substrate in 0.9% NaCl at both temperatures. The corrosion rate on the samples with the TiN coating in 0.9% NaCl was 8.3 times lower at 25 °C, and 2.25 times lower at 36 °C. The TiN coating provides 87.96% protection at 25 °C, and 55.62% protection at 36 °C (Table 1).

Table 1. Corrosion parameters obtained by DC techniques.

Sample	*T*, °C	E_{corr}, mV vs. SCE	v_{cor}, µA/y	j_{cor}, µA/cm^2	R_p, Ω/cm^2	η, %
CoCrMo	25 ± 1	−700 ± 0.065	6.59 ± 0.027	0.641 ± 0.029	$6.43 \times 10^3 \pm 0.279$	
	36 ± 1	−240 ± 0.030	3.38 ± 0.038	0.328 ± 0.036	$17.98 \times 10^3 \pm 0.174$	
TiN/CoCrMo	25 ± 1	−592 ± 0.072	0.793 ± 0.046	0.117 ± 0.049	$375 \times 10^3 \pm 0.345$	87.96
	36 ± 1	−190 ± 0.006	1.50 ± 0.051	0.222 ± 0.053	$301 \times 10^3 \pm 0.231$	55.62

All values are denoted as mean ± SD for n = 5.

Figure 3 shows the CoCrMo substrate after DC testing at 25 °C and 36 °C. The corrosion current density, as well as the corrosion rate for the CoCrMo substrate in a 0.9% NaCl solution is higher at 25 °C than at 36 °C, which can be explained by the presence of more stable oxide layers at higher temperatures.

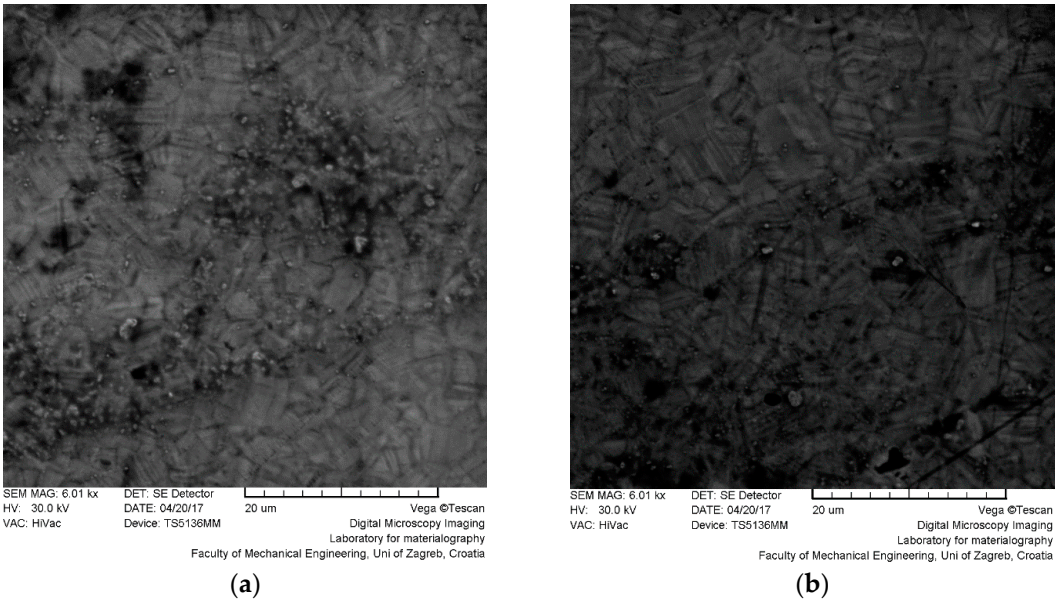

Figure 3. SEM images of: (**a**) CoCrMo substrate after DC polarization at 25 °C; and (**b**) 36 °C.

Figure 4 shows the corrosion damage in the TiN coating after DC testing at 25 °C and 36 °C. White areas present the created corrosion products, which are more visible at 36 °C. This was also confirmed with a lower coating resistance as shown in Table 1.

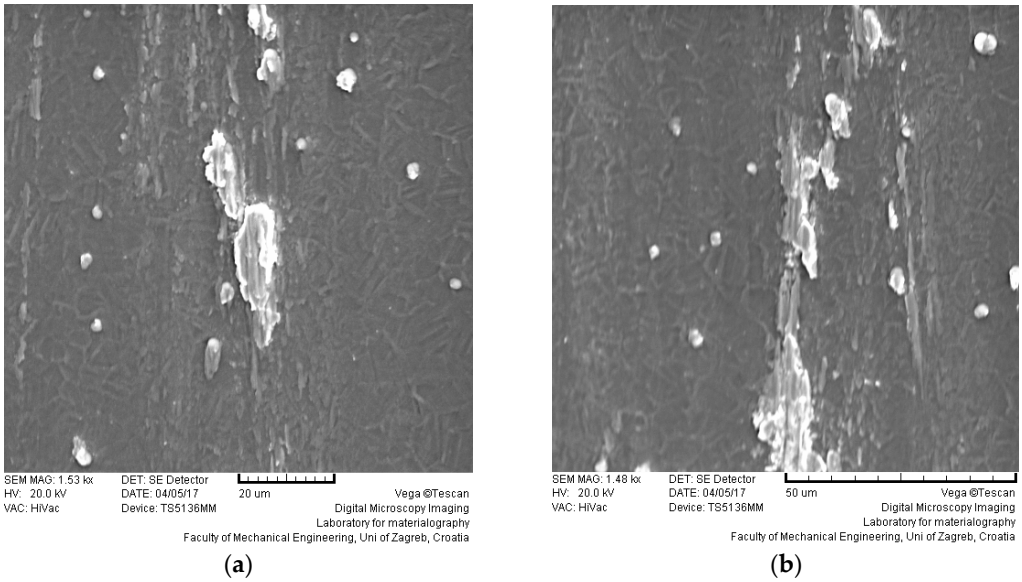

Figure 4. SEM image of TiN coatings after DC polarization at (**a**) 25 °C; and (**b**) 36 °C.

3.3. Electrochemical AC Results

The electrochemical behaviour at the coating/electrolyte interface is the key factor in understanding the protective properties of the TiN coating and CoCrMo alloy. The impedance spectrum for a specific electrochemical system can be connected with one or more equivalent electrical models. The electrode/electrolyte interface can be described with an equivalent electrical model which contains a specific combination of resistors and capacitors. The comparison of the test results with a specific model of the equivalent electrical model presents the base for interpreting physical processes. Figures 5–8 show the results recorded in the electrolyte solution and the results obtained by

mathematical synchronization with the equivalent electrical models. The values of the circuit elements, obtained by synchronization of the measurement data with the theoretical function of the equivalent electrical model, are shown in Tables 2 and 3.

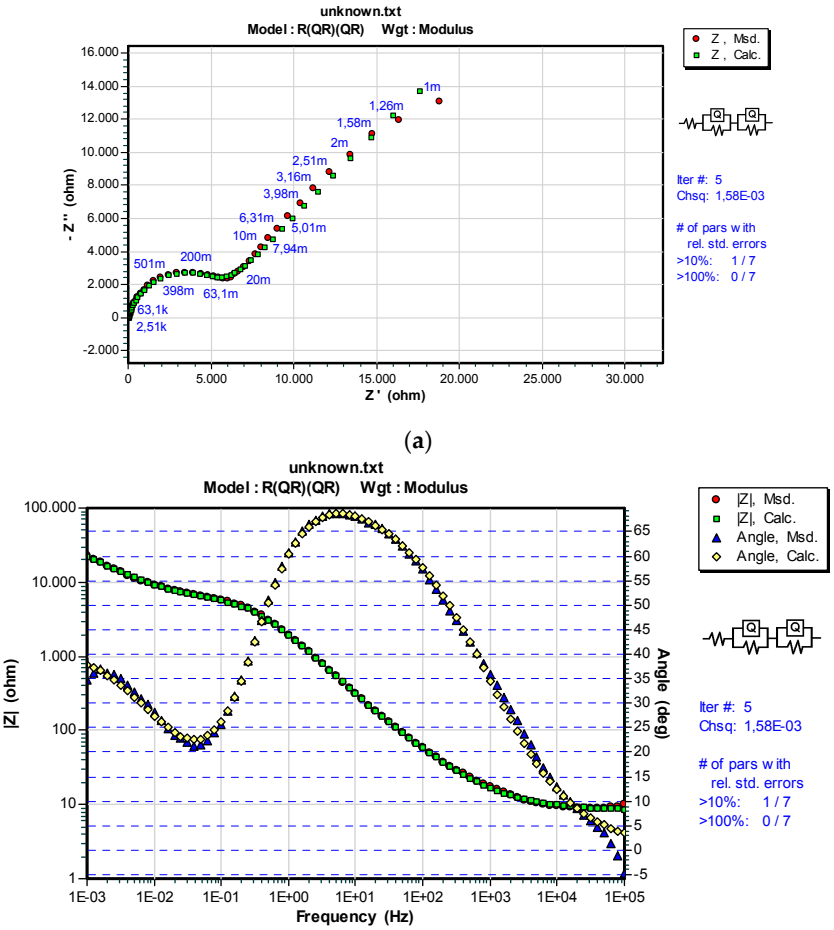

Figure 5. Nyquist (**a**) and Bode (**b**) illustrations of the impedance spectrums recorded in a 0.9% NaCl solution, at 25 °C after 1 h of stabilization at the open circuit potential and equivalent electric model used in the impedance spectrum analysis of the CoCrMo alloy.

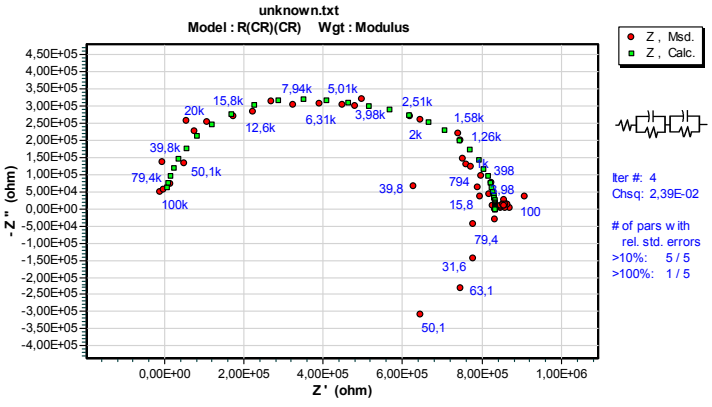

Figure 6. *Cont.*

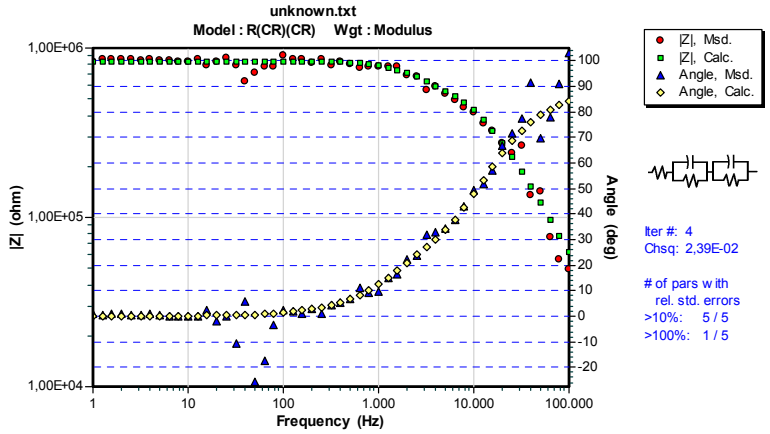

(**b**)

Figure 6. Nyquist (**a**) and Bode (**b**) illustrations of the impedance spectrums recorded in a 0.9% NaCl solution, at 36 °C after 1 h of stabilization at the open circuit potential and equivalent electric model used in the impedance spectrum analysis of the CoCrMo alloy.

EIS measurement results are shown with Nyquist and Bode graphs. The R(QR)(QR) (equivalent electric circuit which consists resistance (R), a combination of the constant phase element (Q), connected in series) model was used for the CoCrMo alloy recorded at 25 °C, whereas the R(CR)(CR) (equivalent electric circuit which consists resistance (R), a combination of the capacity (C) connected in series) model was used for the same alloy recorded at 36 °C. In the model applied for the CoCrMo alloy surface, the equivalent electric circuit consists of the electrolyte solution resistance (R_S), connected in series with a combination of the constant phase element (CPE_{ox}), or in the case of an increased temperature of the capacity (C_{ox}) and resistance (R_{ox}) of the layer oxide with the constant phase element (CPE_{dl}), or in the case of an increased temperature of the double layer capacity (C_{dl}) and the resistance to the charge transfer (R_{ct}). The parameter values of the AC circuit model, obtained by synchronization of the impedance data measured for the CoCrMo alloy system, are shown in Table 2.

Table 2. The electrochemical impedance spectroscopy (EIS) parameters for the CoCrMo alloy obtained in 0.9 % NaCl.

Sample	R_s, $\Omega \cdot cm^2$	CPE_{ox}, $S \cdot s^n \cdot cm^2$	n_{ox}	C_{ox}, F/cm^2	R_{ox}, $\Omega \cdot cm^2$	CPE_{dl}, $S \cdot s^n \cdot cm^2$	n_{dl}	C_{dl}, F/cm^2	R_{ct}, $\Omega \cdot cm^2$
CoCrMo (25 ± 1) °C	8.25	1.10×10^{-4}	0.91	-	4.81×10^3	8.79×10^{-4}	0.56	-	$2.11 \times 10^5 \pm 0.085$
CoCrMo (36 ± 1) °C	22.12	-	-	2.12×10^{-10}	3.41×10^5	-	-	2.90×10^{-11}	$4.92 \times 10^5 \pm 0.048$

All values are denoted as mean ± SD for n = 5.

Where:

R_s—electrolyte solution resistance between the working electrode and the reference electrode in a three-electrode cell;

R_{ox}—the resistance of the oxide layer;

R_{ct}—polarization resistance or resistance to charge transfer on the electrode/electrolyte interface;

C_{dl}—double layer capacity at the electrode/electrolyte interface;

C_{ox}—capacity of the oxide layer;

CPE_{dl} or Constant Phase Element—modified phase element introduced to improve the representation of the impedance by the model, and depends on the empirical constant for the determination of n behaviour which represents the capacitive properties of the layers, and is in the range from 0 to 1. If n = 0, CPE will act as a resistor, and if n = 1, CPE will act as a capacitor;

CPE_{ox}—modified phase elements for the impedance of the oxide layer. Determination of CPE_{ox} is provided through empirical constants n_{ox}.

In the samples of the CoCrMo alloy at 36 °C, $\log|Z|$ is linear with $\log f$, which represents significant capacity behaviour at the electrode/electrolyte interface, typical for passive alloys [22]. Almost an ideal capacity property of the CoCrMo alloy at 36 °C is also visible in the amount of the phase angle near −90 °C in the high frequency range. The impedance in the low frequency range around 1 MΩ·cm^2 was recorded for the CoCrMo alloy sample at 36 °C. The exponent value (n) near 1 indicates the capacity behaviour of the CoCrMo alloy at 25 °C, whereas the oxide layer capacity C_{ox} for the CoCrMo alloy at 36 °C is 2.12×10^{-10} F/cm^2. The bare oxide surface resistance (R_{ox}) is higher for the alloy recorded at 36 °C in comparison with the layer resistance for the alloy recorded at 25 °C, which indicates good corrosion resistance even at a higher temperature. The value (R_{ct}) is of the same order of magnitude for the CoCrMo alloy at both temperatures.

The R(Q(R(CR))) model was used on the TiN/CoCrMo alloy at both 25 °C and 36 °C. The TiN/CoCrMo surface was modelled by the Randles model and a modified circuit containing a double layer capacity (C_{dl}) and resistance to charge transfer (R_{ct}) component, as well as an embedded parallel combination of resistance (R_{coat}) and *CPE* (CPE_{coat}), which describes the coating efficiency. The modified circuit is a result of the response which contains two peaks of the phase angle concerning the coating presence on the electrode surface. The parameter values of the AC circuit model, obtained by synchronization of the impedance data measured for the TiN/CoCrMo alloy system, are shown in Figures 7 and 8, and Table 3.

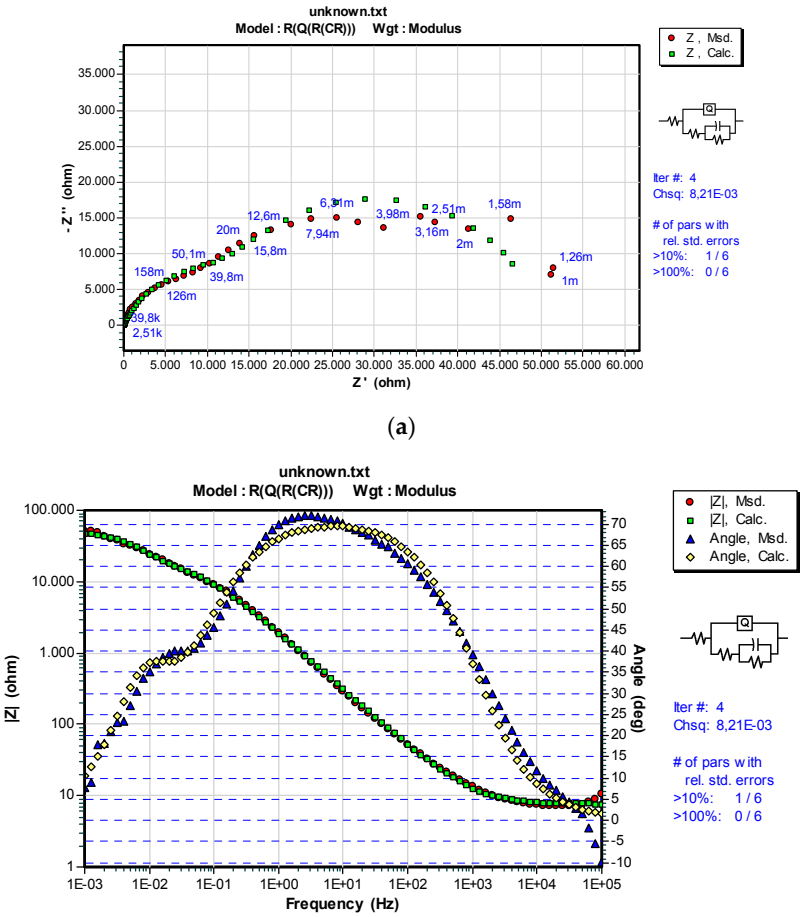

Figure 7. Nyquist (**a**) and Bode (**b**) illustrations of the impedance spectrums recorded in a 0.9% NaCl solution, at 25 °C after 1 h of stabilization at the open circuit potential and equivalent electric model used in the impedance spectrum analysis of the TiN/CoCrMo alloy.

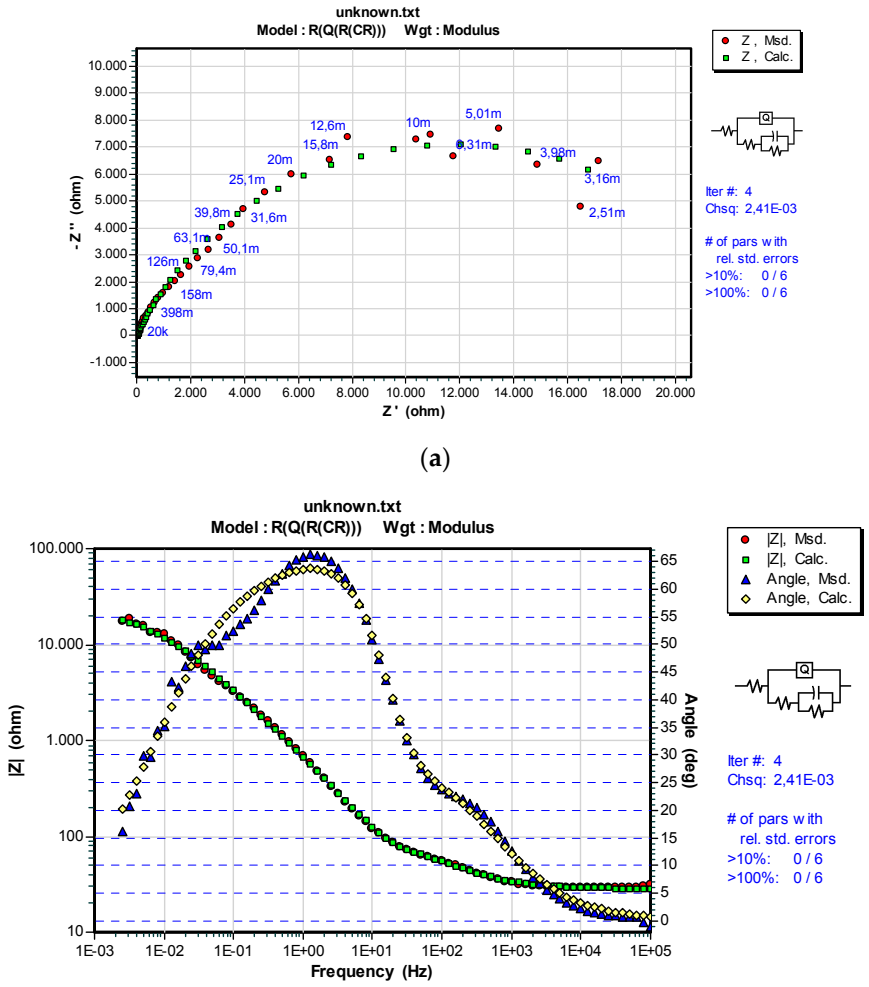

Figure 8. Nyquist (**a**) and Bode (**b**) illustrations of the impedance spectrums recorded in a 0.9% NaCl solution, at 36 °C after 1 h of stabilization at the open circuit potential and equivalent electric model used in the impedance spectrum analysis of the TiN/CoCrMo alloy.

Table 3. EIS parameters for the CoCrMo alloy with an applied TiN coating obtained in 0.9% NaCl.

Sample	R_s, Ω·cm^2	CPE_{coat}, S s^n cm^2	n_{coat}	C_{coat}, F/cm^2	R_{coat}, Ω·cm^2	CPE_{dl}, S s^n cm^2	n_{dl}	C_{dl}, F/cm^2	R_{ct}, Ω·cm^2
TiN (25 ± 1) °C	7.59	1.20×10^{-4}	0.79	-	2.17×10^4	-	-	8.99×10^{-4}	$2.84 \times 10^4 \pm 0.057$
TiN (36 ± 1) °C	28.26	3.32×10^{-4}	0.66	-	90.78	-	-	6.93×10^{-5}	$2.38 \times 10^4 \pm 0.045$

All values are denoted as mean ± SD for n = 5.

Where:

R_s—electrolyte solution resistance between the working electrode and the reference electrode in a three-electrode cell;

R_{ct}—polarization resistance or resistance to charge transfer on the electrode/electrolyte interface;

R_{coat}—the resistance of the coating;

C_{dl}—double layer capacity at the electrode/electrolyte interface;

C_{coat}—capacity of the coating;

CPE_{dl} or Constant Phase Element—modified phase element introduced to improve the representation of the impedance by the model, and depends on the empirical constant for the

determination of n behaviour which represents the capacitive properties of the layers, and is in the range from 0 to 1. If $n = 0$, CPE will act as a resistor, and if $n = 1$, CPE will act as a capacitor;

CPE_{coat}—modified phase elements for the coating impedance. The determination of CPE_{coat} is provided through the empirical constants n_{coat}.

As can be seen from the phase angle illustrations in Figures 7 and 8, the coated surfaces show low phase angles and double peaks typical for coatings. For the coated alloy, the outer part of the circuit (R_{coat} and CPE_{coat}) explains the response in the high frequency range for all coated samples, where CPE_{coat} is connected to the peak in the high frequency range of the phase angle illustration. The inner part of the circuit (R_{ct} and CPE_{dl}) explains the response in the low frequency range for all coated samples, where CPE_{dl} is connected to the peak in the low frequency range of the phase angle illustration. The two peaks are in close vicinity, and they appear in the 0.01–100 Hz frequency range. The peak in the high frequency range appears due to electrochemical interaction at the coating/electrolyte interface, whereas the peak in the low frequency range appears due to electrochemical interaction at the coating/electrode interface [23]. In the frequency range of approximately 1 Hz, the phase angle has a maximum value of approximately 70°. At high frequencies, the phase angle is near 0°, and the Ohm resistance is dominant over the impedance in that range. Therefore, it can be concluded that the sample with the TiN coating, exposed to a 0.9% NaCl solution, is in a passive state. The appearance of the other time constant, connected with the electrode/electrolyte interface, can be ascribed to the cracks created on the coating after the coating has been exposed to the electrolyte solution for a certain time in both cases. The model of the equivalent circuit for the coating shows high heterogeneity ($n < 0.8$) of the coating/electrode interface surface in comparison with the oxide on the bare metal surface. Resistance to charge transfer (R_{ct}) for the TiN coating is the same for both temperatures tested.

The differences in impedance and the phase angle show corrosion damages on the metal with and without the coating. Higher impedance values and a wider peak response of the phase angle on the bare alloy surfaces exposed to a 0.9% NaCl solution imply higher corrosion resistance of these surfaces. However, during the exposure to high temperature, the phase angles shift, and the impedance values increase significantly, which indicates additional passivation of the CoCrMo alloy surface under these conditions. This is also visible in the parameter values of the model for the oxide surface where the oxide layer resistance increases with the temperature increase. With the development of localised corrosion, corrosion products, including oxide compounds, can temporarily block micropores at the surface, which are explained by T.M. Yue et al. [24]. This process slows down the corrosion rate, which is evident in the increase of n, as in the case of the CoCrMo alloy where we measured the oxide layer capacity (C_{ox}) at the increased temperature. The compact structure of the oxide layer enables corrosion products to close the cracks of micro-corrosion damage more efficiently. The formed oxide layers have good mechanical and physical-chemical properties, as well as adhesion to the substrate. Good oxide layers have Pilling-Bedworth ratios (i.e., volume proportions between the oxide and oxidised metal) between 1 and 2.5, for Cr/Cr_2O_3 and Co/Co_2O_3, and the ones formed on CoCrMo are equal to 2.02 and 2.46, respectively.

In their research, numerous authors have studied the elution of metal ions in a NaCl solution, and have consequently concluded that a TiN coating provides good protective properties to the CoCrMo substrate. However, electrochemical testing has proved that thin and porous TiN coatings cause accelerated pitting corrosion [15,17].

The impedance behaviour of a TiN coating in a 0.9% NaCl solution is very similar to the oxide surface behaviour, and can be connected with the heterogeneity of a thin TiN coating. Changes in the porosity index (n), which occur with time lapse, indicate poorer corrosion resistance at a higher temperature for TiN coating samples. For the CoCrMo alloy at 25 °C, n is 0.91, which is near 1, and indicates a strong capacity response at the electrolyte/coating interface. There is an evident fall in the n value for the TiN coating sample, which means that the capacity interface expands, and the obtained results match the results obtained by Liu et al. [25]. The present microporosity in the TiN coating causes stronger corrosion attacks at the coating/electrode interface. When the TiN coating

is exposed to a higher temperature, the n value drops significantly to 0.66, which confirms stronger corrosion attacks at the coating surface, and which is in accordance with the results obtained by Bolton and Hu [18].

The charge transfer resistance (R_{ct}) at the electrode/electrolyte interface is an indicator of the electrochemical reaction rate. The polarization resistance is the same resistance as the charge transfer resistance at the electrode/electrolyte interface. The R_p obtained by the DC testing shows better properties of the TiN coating in comparison with the CoCrMo alloy at both temperatures, whereas the values obtained by the AC testing illustrate that the TiN coating samples show a higher release level of metal ions into the solution than the samples without the coating, as can be concluded from the lower polarization resistance (R_{ct}). The results of this research show that the electrochemical behaviour of the TiN coating is strongly affected by the coating microstructure, coating porosity, and coating deposition conditions, as confirmed by other authors as well [18]. TiN coatings which consist of columnar crystallites provided straight boundaries for the diffusion of oxygen [26].

The measurement results of the polarization resistance R_p and charge transfer resistance R_{ct} were statistically analysed. In order to determine the effect of temperature on the polarization resistance R_p and charge transfer resistance R_{ct}, the sample groups (CoCrMo, TiN) at different temperatures (25 $\pm$ 1, 36 $\pm$ 1) °C were compared by using the F-test and the T test.

In a comparison between the R_p and R_{ct} standard deviations, using the F-test, all p-values (3.14, 1.60, 2.57, 2.23) achieved on the sample groups at different temperatures are greater than the reasonable choice of $\alpha = 0.05$. The null hypothesis which stated that the standard deviations of R_p and R_{ct} are equal cannot be rejected. These data do not provide enough evidence to claim that the polarization resistance R_p and charge transfer resistance R_{ct} achieved on the two sample groups at different temperatures have unequal standard deviations. It can be concluded that the temperature does not significantly affect the precision of the polarization resistance R_p and charge transfer resistance R_{ct} measurement results.

Furthermore, the measurement results were analysed using the T test. In comparison between the R_p and R_{ct} measurement results, all p-values ($p = 0.000$) achieved on the sample groups at different temperatures are less than reasonable choices of the α levels ($\alpha = 0.05$). It can be concluded that higher temperatures cause greater polarization resistance R_p and charge transfer resistance R_{ct} on the CoCrMo samples, and an opposite effect on the TiN samples. A greater temperature effect was observed on the CoCrMo sample. A statistical comparison between the R_p and R_{ct} measurement results was not necessary due to the plainly visible significant differences between their results.

4. Conclusions

The electrochemical and morphological study of the TiN coatings and CoCrMo substrate permitted an estimation of their behaviour in a 0.9% NaCl solution at 25 °C and 36 °C, and an observation of the properties of the coatings' surfaces after the corrosion attack. The results obtained can be summarized as follows:

- SEM analysis of the cross-section proved the uniform thickness and density, and the topography analysis of the surface determined the presence of micrometal TiN drops.
- DC testing proved that the TiN/CoCrMo and CoCrMo samples have more positive values of the corrosion potential at 36 °C in comparison with 25 °C.
- The TiN coating shows better chemical stability at both temperatures in comparison with the CoCrMo alloy in a 0.9% NaCl solution.
- AC electrochemical testing shows higher values of the polarization resistance (R_{ct}) for the CoCrMo alloy in comparison with the TiN coating in a 0.9% NaCl solution at both temperatures, which can be explained by the formation of more stable oxide layers on the CoCrMo alloy.
- SEM/EDS micrographs revealed that the surface morphology of the TiN layers after linear polarization is highly heterogeneous with corrosion products.

- The corrosion rate on the samples with the TiN coating in 0.9% NaCl was 8.3 times lower at 25 °C, and 2.25 times lower at 36 °C than CoCrMo alloy without coating.
- The TiN coating provides 87.96% protection at 25 °C, and 55.62% protection at 36 °C.

The physical-chemical properties of the TiN coating depend significantly on the temperature, time, and deposition rate. Better TiN coating properties can be achieved by optimizing these parameters, which shall be the continuation of this research.

Further research is necessary to fully explain the influence of the PACVD process parameters on better adhesion of the TiN coating on the CoCrMo medical alloy. It is necessary to define the thickness, hardness, and roughness of the surface that can provide better adhesion of the coating—the substrate system, and protect the substrate from excessive wear. Additional research may lead to dynamic tests of a PACVD coated femoral head.

Future work will include studies regarding the protein effect on Hank's solution and Ringer's solution.

Acknowledgments: This research did not receive any specific grant from funding agencies in the public, commercial, or not-for-profit sectors.

Author Contributions: Suzana Jakovljević and Vesna Alar conceived and designed the experiments. Vesna Alar performed the DC electrochemical measurements and analyzed the data. Antonio Ivanković performed the EIS measurements and analyzed the data. Suzana Jakovljević performed SEM and EDS analyses and wrote the paper.

Conflicts of Interest: The authors declare no conflict of interest.

References

1. Geetha, M.; Singh, A.K.; Asokamani, R.; Gogia, A.K. Ti based biomaterials, the ultimate choice for orthopaedic implants—A review. *Prog. Mater. Sci.* **2009**, *54*, 397–425. [CrossRef]
2. Milošev, I. CoCrMo alloy for biomedical applications. In *Biomedical Applications*; Djokic, S., Ed.; Springer US: New York, NY, USA, 2012; Volume 55, pp. 1–72.
3. Hu, P.; Liu, R.; McRae, G. Investigation of wear and corrosion of a high-carbon stellite alloy for hip implants. *J. Mater. Eng. Perform.* **2014**, *23*, 1223–1230. [CrossRef]
4. Bellefontaine, G. The Corrosion of CoCrMo Alloys for Biomedical Application. Master's Thesis, University of Birmingham, Birmingham, UK, 2010.
5. Yan, Y.; Neville, A.; Dowson, D. Tribo-corrosion properties of cobalt-based medical implant alloys in simulated biological environments. *Wear* **2007**, *263*, 1417–1422. [CrossRef]
6. Liao, Y.; Hoffman, E.; Wimmer, M.; Fischer, A.; Jacobs, J.; Marks, L. CoCrMo metal-on-metal hip replacements. *Phys. Chem. Chem. Phys.* **2013**, *15*, 746–756. [CrossRef] [PubMed]
7. Posada, O.M.; Tate, R.J.; Meek, R.M.D.; Grant, M.H. In vitro analyses of the toxicity, immunological, and gene expression effects of cobalt-chromium alloy wear debris and Co ions derived from metal-on-metal hip implants. *Lubricants* **2015**, *3*, 539–568. [CrossRef]
8. Okazaki, Y.; Gotoh, E. Comparison of metal release from various metallic biomaterials in vitro. *Biomaterials* **2005**, *26*, 11–21. [CrossRef] [PubMed]
9. Ribeiro, M.; Monteiro, F.J.; Ferraz, M.P. Infection of orthopedic implants with emphasis on bacterial adhesion process and techniques used in studying bacterial-material interactions. *Biomatter* **2012**, *4*, 176–194. [CrossRef] [PubMed]
10. Lewis, A.C.; Kilburn, M.R.; Heard, P.J.; Scott, T.B.; Hallam, K.R.; Allen, G.C.; Learmonth, I.D. The Entrapment of corrosion products from CoCr implant alloys in the deposits of calcium phosphate: A comparison of serum, synovial fluid, albumin, EDTA, and water. *J. Orthop. Res.* **2006**, *24*, 1587–1596. [CrossRef] [PubMed]
11. Ching, H.A.; Choudhury, D.; Nine, J.; Osman, N.A.A. Effects of surface coating on reducing friction and wear of orthopaedic implants. *Sci. Technol. Adv. Mater.* **2014**, *15*, 014402. [CrossRef] [PubMed]
12. Gotman, I.; Gutmanas, E.Y. Titanium nitride-based coatings on implantable medical devices. *Adv. Biomater. Devices Med.* **2014**, *1*, 53–73.
13. Scarano, A.; Piattelli, M.; Vrespa, G.; Caputi, S.; Piattelli, A. Bacterial adhesion on titanium nitride-coated and uncoated implants: An in vivo human study. *J. Oral Implantol.* **2003**, *29*, 80–85. [CrossRef]

14. Van Hove, R.P.; Sierevelt, I.N.; van Royen, B.J.; Nolte, P.A. Titanium-nitride coating of orthopaedic implants: A review of the literature. *BioMed Res. Int.* **2015**, *2015*, 485975. [CrossRef] [PubMed]
15. Türkan, U.; Öztürk, O.; Eroğlu, A.E. Metal ion release from TiN coated CoCrMo orthopedic implant material. *Surf. Coat. Technol.* **2006**, *200*, 5020–5027. [CrossRef]
16. Wisbey, A.; Gregson, P.J.; Tuke, M. Application of PVD TiN coating to CoCrMo based surgical implants. *Biomaterials* **1987**, *8*, 477–480. [CrossRef]
17. Goldberg, J.R.; Gilbert, J.T. The electrochemical and mechanical behavior of passivated and TiN/AlN-coated CoCrMo and Ti6Al4V alloys. *Biomaterials* **2004**, *25*, 851–864. [CrossRef]
18. Bolton, J.; Hu, X. In vitro corrosion testing of PVD coatings applied to a surgical grade CoCrMo alloy. *J. Mater. Sci. Mater. Med.* **2002**, *13*, 567–574. [CrossRef] [PubMed]
19. Dicu, M.M.; Gleizes, A.; Demetrescu, I. Titanium dioxide MIOCVD coating on CoCr Alloy and its properties in compere with phosphate coatings. In Proceedings of the 14th Nordic-Baltic Conference on Biomedical Engineeing and Medical Physics, Riga, Latvia, 16–20 June 2008; Katashev, A., Dekhtyar, Y., Spigulis, J., Eds.; Springer: Heidelberg/Berlin, Germany, 2008; pp. 26–29.
20. Creus, J.; Mazille, H.; Idrissi, H. Porosity evaluation of protective coatings onto steel, through electrochemical techniques. *Surf. Coat. Technol.* **2000**, *130*, 224–232. [CrossRef]
21. Ahn, S.H.; Lee, J.H.; Kim, J.G. Localized corrosion mechanisms of the multilayered coatings related to growth defects. *Surf. Coat. Technol.* **2004**, *177*, 638–644. [CrossRef]
22. Li, M.C.; Luo, S.Z.; Zeng, C.L. Corrosion behavior of TiN coated type 316 stainless steel in simulated PEMFC environments. *Corros. Sci.* **2004**, *46*, 1369–1380. [CrossRef]
23. Zhong, C.; Tang, X.; Cheng, Y.F. Corrosion of steel under the defected coating studied by localized electrochemical impedance spectroscopy. *Electrochim. Acta* **2008**, *53*, 4740. [CrossRef]
24. Yue, T.M.; Yu, J.K.; Man, H.C. The effect of excimer laser surface treatment on pitting corrosion resistance of 316LS stainless steel. *Surf. Coat. Technol.* **2001**, *137*, 65–71. [CrossRef]
25. Liu, C.; Chu, P.K.; Lin, G.; Yang, D. Effects of Ti/TiN multilayer on corrosion resistance of nickel–titanium orthodontic brackets in artificial saliva. *Corros. Sci.* **2007**, *49*, 3783–3796. [CrossRef]
26. Liu, C.; Bi, Q.; Leyland, A.; Matthews, A. An electrochemical impedance spectroscopy study of the corrosion behaviour of PVD coated steels in 0.5 N NaCl aqueous solution: Part II.: EIS interpretation of corrosion behaviour. *Corros. Sci.* **2003**, *45*, 1257–1273. [CrossRef]